DFT-Guided Additive Design for $BaTiO_3$-Based MLCCs Exhibiting Excellent Insulation Reliability

Gi Joo Bang,* Hyo-Ki Hong, Seong Hun Kim, Juhun Park, Kang-Sahn Kim, and Giwoong Ha*

Materials Computation Group, Corporate R&D Institute, Samsung Electro-Mechanics Co., Ltd., Suwon, Gyeonggi-Do, 16674, Republic of Korea

Corresponding Author

**E-mail: gijoo.bang@samsung.com*

**E-mail: giwoong.ha@samsung.com*

Computational details

Spin-polarized density functional theory (DFT) methods were performed using the Vienna Ab-initio Simulation Package (VASP) with projector-augmented wave (PAW) pseudopotentials.[1–3] The generalized gradient approximation (GGA) with the Perdew-Burke-Ernzerhof (PBE) functional[4] was employed for the exchange-correlation energy. A 3 × 3 × 3 supercell of cubic perovskite $BaTiO_3$ was used, and atomic positions were constrained for all atoms beyond a 4 Å radius from the dopant or oxygen vacancy (V_O). In single-doped $BaTiO_3$, a dopant atom replaced one atom at either the A-site or B-site, corresponding to a doping concentration of 3.7 at%. For co-doped $BaTiO_3$, both two dopant atoms were simultaneously substituted within the same supercell. Based on our calculations revealing strong interactions between dopants and V_O within 2nd nearest neighbor distance (Figure S8), we considered only configurations where all dopants were located within 2nd nearest neighbor sites of V_O for co-doped $BaTiO_3$ with V_O. Structural optimization was performed until the energy difference and residual atomic forces converged to less than 10^{-5} eV and 0.05 eV/Å, respectively. A plane-wave cutoff energy of 500 eV was used. A 2 × 2 × 2 k-point mesh generated using the Monkhorst-Pack[5] was employed to sample the Brillouin zone. An on-site Coulomb repulsion correction (Hubbard U) was applied to the highly localized Ti 3*d*, Mn 3*d*, and Ce 4*f* orbitals, with values of 4 eV, 5.04 eV and 5 eV, respectively. For heavy rare-earth elements (Tb, Dy, and Er), we used pseudopotentials treating 4*f* orbitals as core states. To investigate the possible oxidation states of Ce within $BaTiO_3$, we employed electron or hole injection in the supercell. Specifically, using the NELECT tag in VASP, electron (hole) injection was conducted by adding (subtracting) electrons in the supercell. The solution energy (E_s) of Ce in $BaTiO_3$ and interaction energy (E_{int}) between the dopant and V_O were calculated following the

methodology described by previous literature.[6–9] The detailed calculation procedures of E_s and E_{int} are described in the following section. For co-doped $BaTiO_3$, the E_{int} between dopant combinations (D_1-D_2) and V_O, was calculated by subtracting the E_{int} of the D_1-D_2 combination from the E_{int} of the entire D_1-D_2-V_O. The error correction of triplet O_2 molecule was performed using the standard enthalpy of the reaction, $H_2(g) + 1/2\ O_2(g) \rightarrow H_2O(g)$, as determined experimentally.[10]

Calculation of E_s and E_{int}

The E_s represents the energy required for a dopant to be incorporate into the A- or B-site of $BaTiO_3$ in a particular doping configuration. When the dopant element possesses a different oxidation state compared with Ba^{2+} or Ti^{4+}, E_s is calculated for all doping configurations that achieve charge compensation through the formation of electron, hole, or vacancies. For example, doping with Ce^{3+} at the A-site results in the formation of $1e^-$ or $0.5V_{Ba}$ or $0.25V_{Ti}$ to maintain charge neutrality. The E_s in each of these doping forms is calculated according to the following equation:

$$(i)\ E_s\left[Ce_{Ba} + e^-\right] = E\left[Ba_{n-1}CeTi_nO_{3n}\right] - E\left[Ba_nTi_nO_{3n}\right] + \mu_{Ba} - \mu_{Ce}$$

$$(ii)\ E_s\left[Ce_{Ba} + 0.5V_{Ba}\right] = E\left[Ba_{n-1}CeTi_nO_{3n} : \Delta n_{e^-} = -1\right] + 0.5E\left[Ba_{n-1}Ti_nO_{3n} : \Delta n_{e^-} = +2\right] - 1.5E\left[Ba_nTi_nO_{3n}\right] + 1.5\mu_{Ba} - \mu_{Ce}$$

$$(iii)\ E_s\left[Ce_{Ba} + 0.25V_{Ti}\right] = E\left[Ba_{n-1}CeTi_nO_{3n} : \Delta n_{e^-} = -1\right] + 0.25E\left[Ba_nTi_{n-1}O_{3n} : \Delta n_{e^-} = +4\right] - 1.25E\left[Ba_nTi_nO_{3n}\right] + \mu_{Ba} + 0.25\mu_{Ti} - \mu_{Ce}$$

where E is the total energy obtained from DFT calculations, μ_i is the chemical potential of element *i*, and Δn_{e^-} is the number of electrons adjusted in the DFT calculation using the NELECT tag in VASP. Because the DFT energies of dopant-substituted and vacancy-formed supercells include contributions from the generation of electrons or holes, this adjustment were conducted to remove those contributions.[6] To calculate the E_s under experimental conditions, we defined five equilibrium conditions and obtained the corresponding μ_i. Specifically, μ_i are determined from reference materials under the following equilibrium conditions: $BaTiO_3$-TiO_2-Ti (Ti-rich & Reducing), $BaTiO_3$-TiO_2-O_2 (Ti-rich & Oxidative), $BaTiO_3$-BaO-O_2 (Ba-rich & Oxidative), $BaTiO_3$-BaO-Ba (Ba-rich & Reducing), and $BaTiO_3$-Ba-Ti (Ba/Ti=1 & Reducing).[6] In addition, Ce_2O_3 is used as the reference material to obtain μ_{Ce}.

The E_{int} represents the interaction energy between the dopants and V_O, indicating the degree of stabilization of V_O induced by the dopant. Assuming Ce doping at the A-site, E_{int} is calculated according to the following equation:

$$E_{int} = E\left[Ba_{n-1}CeTi_nO_{3n-1} : \Delta n_{e^-} = -3\right] - E\left[Ba_{n-1}CeTi_nO_{3n} : \Delta n_{e^-} = -1\right] - E\left[Ba_{n-1}Ti_nO_{3n}\right]$$

where the first three terms represent the energies of Ce_{Ba}-doped $BaTiO_3$ with V_O, Ce_{Ba}-doped $BaTiO_3$, and $BaTiO_3$ with V_O, respectively, and the last term represents the energy of pristine $BaTiO_3$. Similar to E_s calculations, contributions to the energy from electron or hole generation were removed by adjusting the number of electrons.[7] In calculations of E_s and E_{int}, the correction terms associated with electron addition/subtraction were not included,

as it can cancel out when the valence band maximum is assumed to be identical for all systems.[6,7]

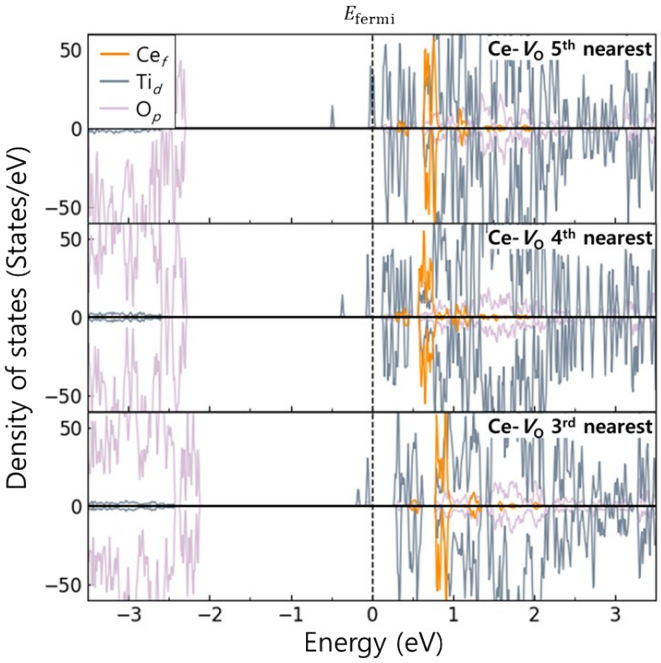

Figure S1. Projected DOS of Ce-doped $BaTiO_3$ with a V_O located at the third, fourth and fifth nearest oxygen site from Ce_{Ti}. The energy states located within the band gap and below the Fermi energy indicate the electron trap states. The Fermi energy is set to 0 eV. The line color indicates the states originating from each atomic orbital (Ce *f*-, Ti *d*-, and O *p*-orbital). Positive (negative) DOS values correspond to majority (minority) spin states. The total DOS is shown in Figure S2.

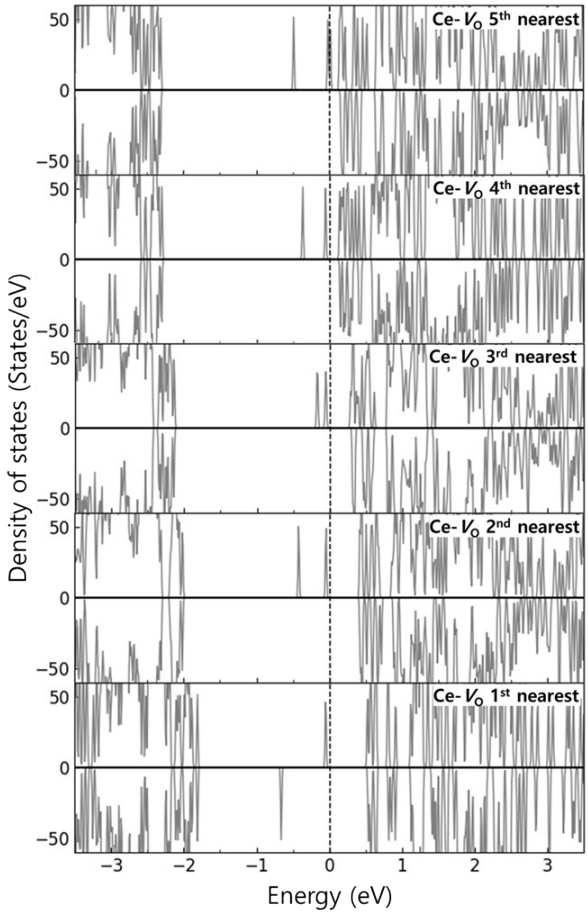

Figure S2. The total DOS of Ce-doped $BaTiO_3$ with V_O. Positive (negative) DOS values correspond to majority (minority) spin states.

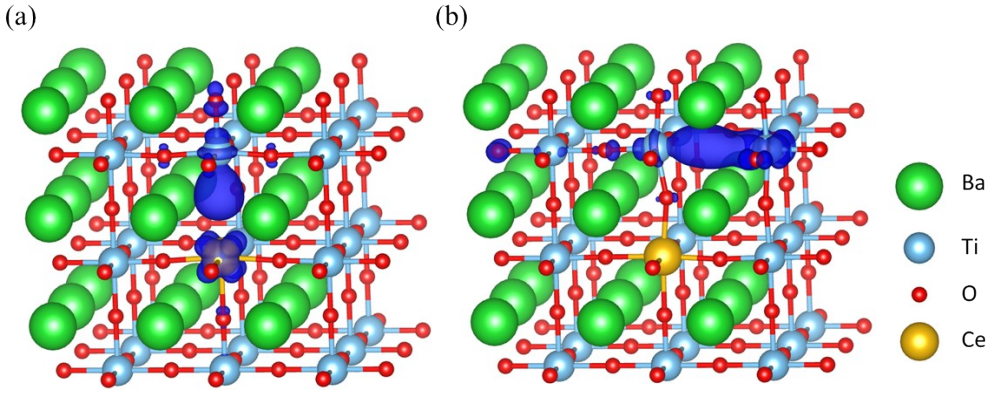

Figure S3. The partial charge density of Ce-doped $BaTiO_3$ with a V_O located at the (a) first and (b) second nearest oxygen site from Ce_{Ti}. The isosurface level is set to 0.005 e/Å^3, and the region of electron localization are represented by the blue lobes.

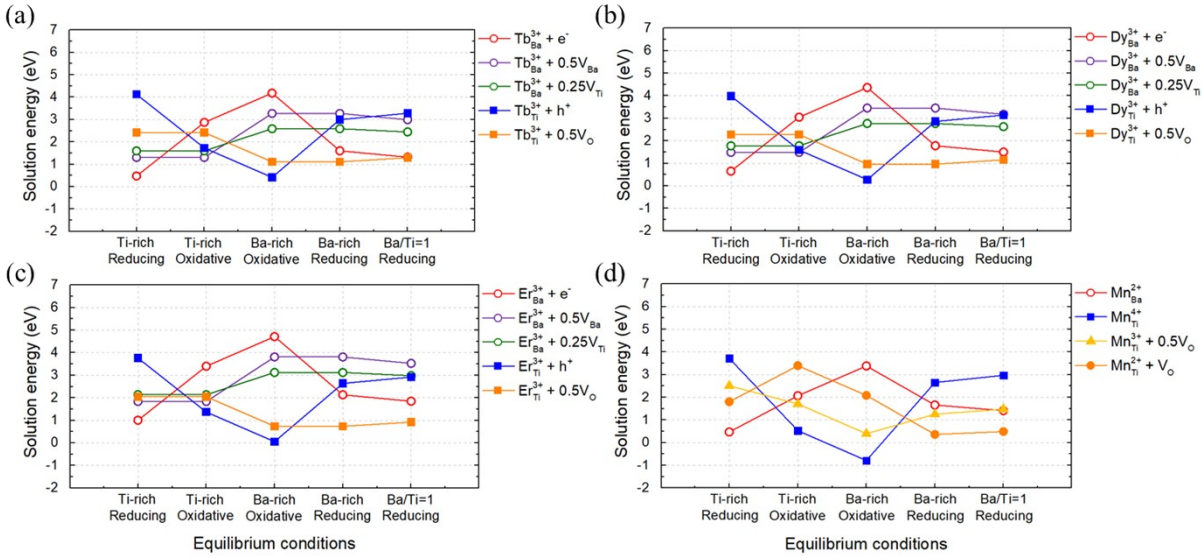

Figure S4. Solution energy (E_s) of (a) Tb, (b) Dy, (c) Er, and (d) Mn at the A-/B-site in $BaTiO_3$.

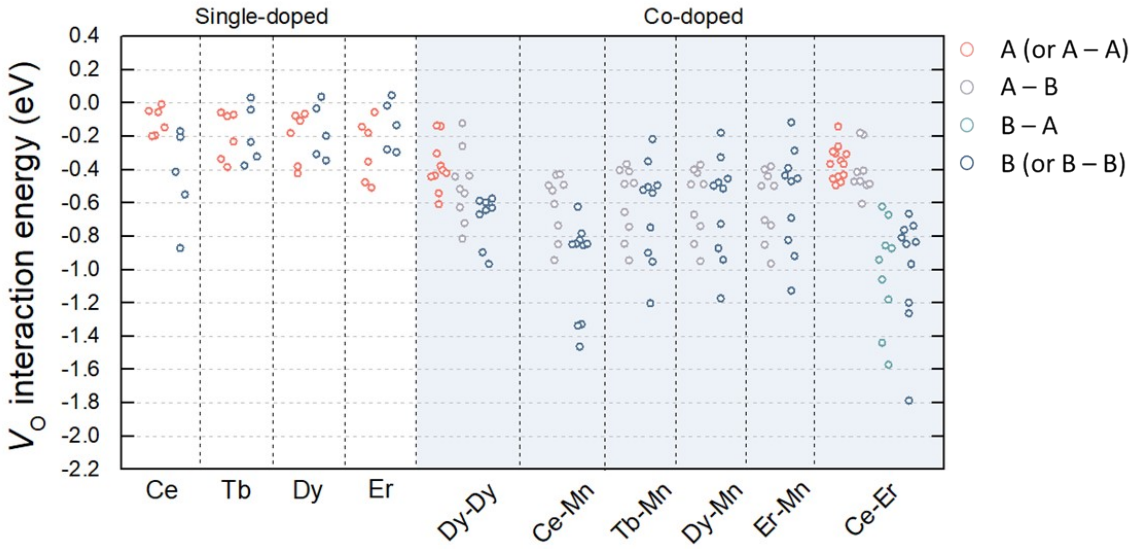

Figure S5. Interaction energy (E_{int}) between various dopants/dopant combinations and V_O. For co-doped $BaTiO_3$, we considered only configurations where all dopants were within the second nearest neighbor of V_O. The data color indicates the doping site for each dopant.

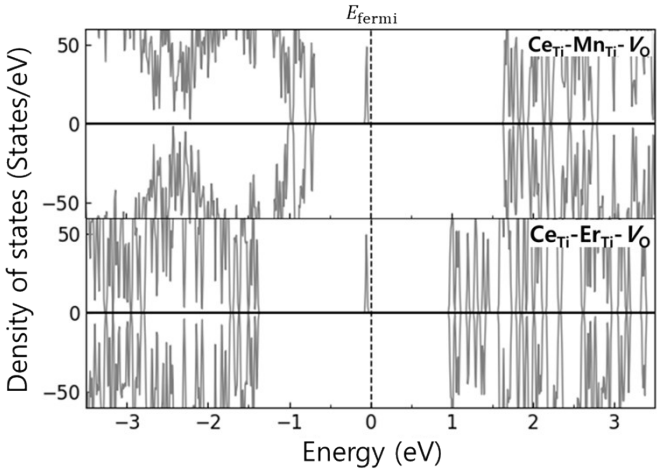

Figure S6. The total DOS of Ce_{Ti}–Mn_{Ti} and Ce_{Ti}–Er_{Ti} doped $BaTiO_3$ with V_O. Positive (negative) DOS values correspond to majority (minority) spin states.

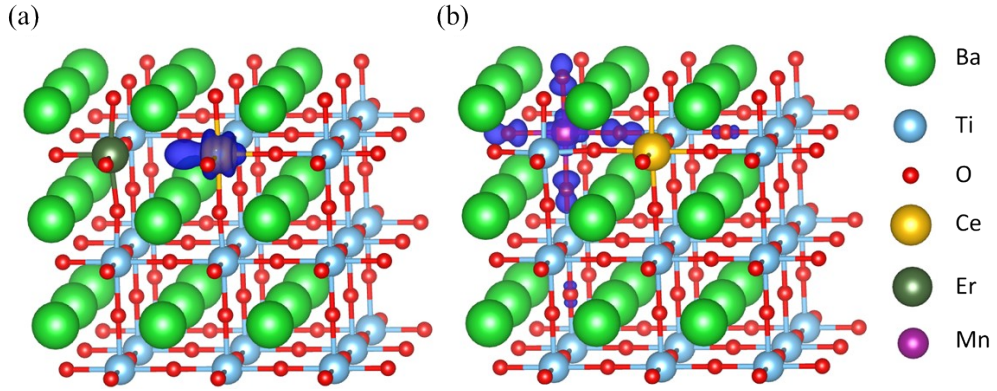

Figure S7. The partial charge density of (a) Ce_{Ti}-Er_{Ti} and (b) Ce_{Ti}-Mn_{Ti} doped $BaTiO_3$ with a V_O. The isosurface level is set to 0.005 e/Å^3, and the region of electron localization are represented by the blue lobes.

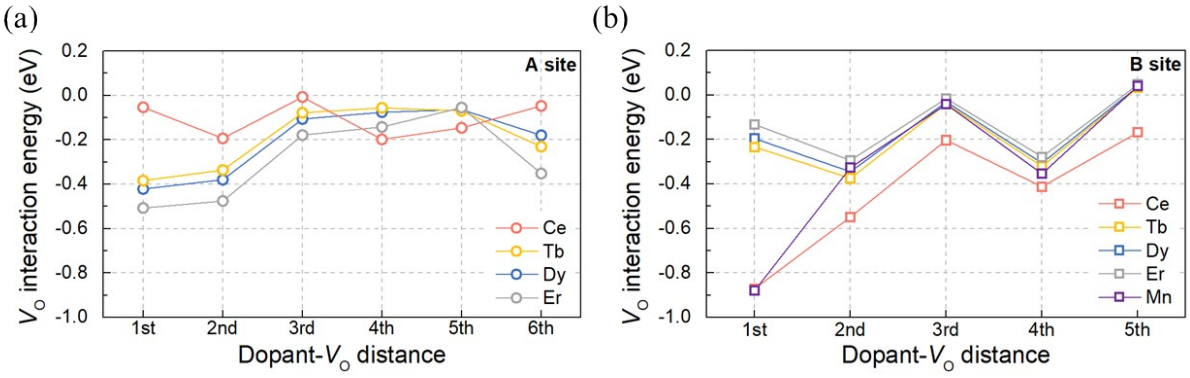

Figure S8. Interaction energy (E_{int}) between V_O and various dopants doped at the (a) A-site, (b) B-site in $BaTiO_3$.

References

1. P. E. Blöchl, *Phys. Rev. B*, 1994, **50**, 17953.
2. G. Kresse and J. Furthmüller, *Comput. Mater. Sci.*, 1996, **6**, 15.
3. G. Kresse and D. Joubert, *Phys. Rev. B*, 1999, **59**, 1758.
4. J. P. Perdew, K. Burke and M. Ernzerhof, *Phys. Rev. Lett.*, 1996, **77**, 3865.
5. H. J. Monkhorst and J. D. Pack, *Phys. Rev. B*, 1976, **13**, 5188.
6. A. Honda, S. Higai, Y. Motoyoshi, N. Wada and H. Takagi, *Trans. Mater. Res. Soc. Jpn.*, 2010, **35**, 217.
7. A. Honda, S. Higai, Y. Motoyoshi, N. Wada and H. Takagi, *Jpn. J. Appl. Phys.*, 2011, **50**, 09NE01.
8. S. Chikada, T. Kubota, A. Honda, S. Higai, Y. Motoyoshi, N. Wada and K. Shiratsuyu, *J. Appl. Phys.*, 2016, **120**, 142122.
9. X. Cheng, Y. Zhen, P. Zhao, K. Hui, M. Xiao, L. Guo, Z. Fu, X. Cao, L. Li and X. Wang, *J. Am. Ceram. Soc.*, 2023, **106**, 5294.
10. A. S. Rosen, J. M. Notestein and R. Q. Snurr, *ACS Catal.*, 2019, **9**, 3576.